SEVENTH FRAMEWORK PROGRAMME

THEME FP7-ICT-2009-C

Instrument	STREP
Project no.	244068
Project acronym	**CROSSTRAP**
Project title	**C**oherently-enhanced **R**aman **O**ne-beam **S**tandoff **S**pectroscopic **TR**acing of **A**irborne **P**ollutants

Deliverable D5.1

Year 1 Periodic Report

Due date of deliverable	month 12
Actual submission date	15/03/2011
Start date of project	01/02/2010
Duration of the project	36 months
Organization name of lead contractor for this deliverable	**TU WIEN**
Dissemination Level	public

SHORT DESCRIPTION:

During the first 12 months of the project we have generated and characterized various types of femtosecond filaments (laser beam self-confinement) as well as femtosecond pulse beams confined inside a capillary (waveguide confinement). We present results obtained with pulses of 4-7 mJ energy at several carrier wavelengths: the fundamental wavelength of an Yb-doped laser around 1030 nm, the signal and idler waves (1.5 and 3.9 μm, respectively) of an optical parametric amplifier (OPA) pumped by a 1-μm Nd/Yb-doped laser combination. The main achievements, reported in this deliverable, are the first observation of efficient lasing from a fs filament and pioneering studies of filamentation and spectral broadening by intense infrared pulses.

1_ INTRODUCTION

The main objective of this work described in Task 1.1 of WP1 (see Description of Work) is to identify potential scenarios for the generation of a backward-propagating laser pulse, either obtained via a reflection from a plasma mirror or from a lasing action in a fs filament. The idea to search for backward lasing from a filament was originally suggested to the meeting of the CROSS TRAP consortium partners in December 2009, before the start of this EU project, by Prof See Leang Chin (Universite Laval) who referred us to his earlier work on the measurement of stimulated emission from atmospheric nitrogen.

The main achievements, reported in this deliverable, are the first observation of efficient lasing from a fs filament and pioneering studies of filamentation and spectral broadening by intense infrared pulses.

The experimental research reported here was conducted by the TU WIEN partner, the theory work and modelling were performed by the ILC MSU partner.

Progress Report CROSS TRAP, WP4
Seed-Oscillator with 500 MHz repetition rate and spectral bandwidth of >20nm

One of the main parts in this project is the application of CARS-spectroscopy to analyze and to determine airborne pollutants, with vibrational states lying in the spectral fingerprint region of wavenumbers of 500 cm^{-1} to 1500 cm^{-1}. Therefore it is an objective of this work package to develop a pulsed laser system capable of delivering a dual output with an optical spectrum in the region around 1030 nm and 1060 nm wavelength, which can then be used, once frequency doubled, as pump and stokes wavelengths for the CARS-process. For maximum CARS-Signal it is highly favored to gain pulses with a temporal duration of <100 fs. This requires a bandwidth of > 20 nm at each center wavelength. In addition these pulses will be picked in bursts of around a few 100 pulses each and further amplified to achieve enough pulse energy for the upcoming applications. To reach a high sampling rate, a high repetition rate has to be realized to ensure that enough signal power is participating in the Raman process due to the small time window of the desired bursts. For this project a repetition frequency on the order of 500 MHz is envisioned.
It is the task of Menlo Systems to develop such a high repetition rate master oscillator and package it into a prototypal, robust structure to ensure long-term operation.

1. Description of the development to achieve high repetition rates

To achieve a repetition rate as high as ~ 500 MHz, the resonator length of the laser oscillator has to be reduced to 60 cm. It is therefore necessary to reduce the optical path length inside the laser cavity considerably. This turns out to be difficult in an all fiber arrangement and we have therefore opted for a hybrid system where the gain material is a relatively short length of Yb doped fiber and all other components are used in free space.
In the following part of this report, steps towards a master oscillator system with the required specifications are described. First, preliminary investigations of the optical setup are described, leading to the final, fully packaged laser system.

1.1. Laser oscillator in all-normal dispersive setup

The first oscillator has been set up as shown in Fig. 1. The pump light is delivered by two fiber-coupled, single-mode pump diodes emitting 650 mW of average power at 974 nm each. The pump light is combined and coupled into the laser ring via a dichroic mirror with a high reflection at 980 nm and high transmission at 1060 nm, offering a sharp edge at 1010 nm in the transmission window. The resonator is set up in an all-normal dispersive design, where a reflection grating with 300 lines/mm is used to assist the modelocking mechanism.

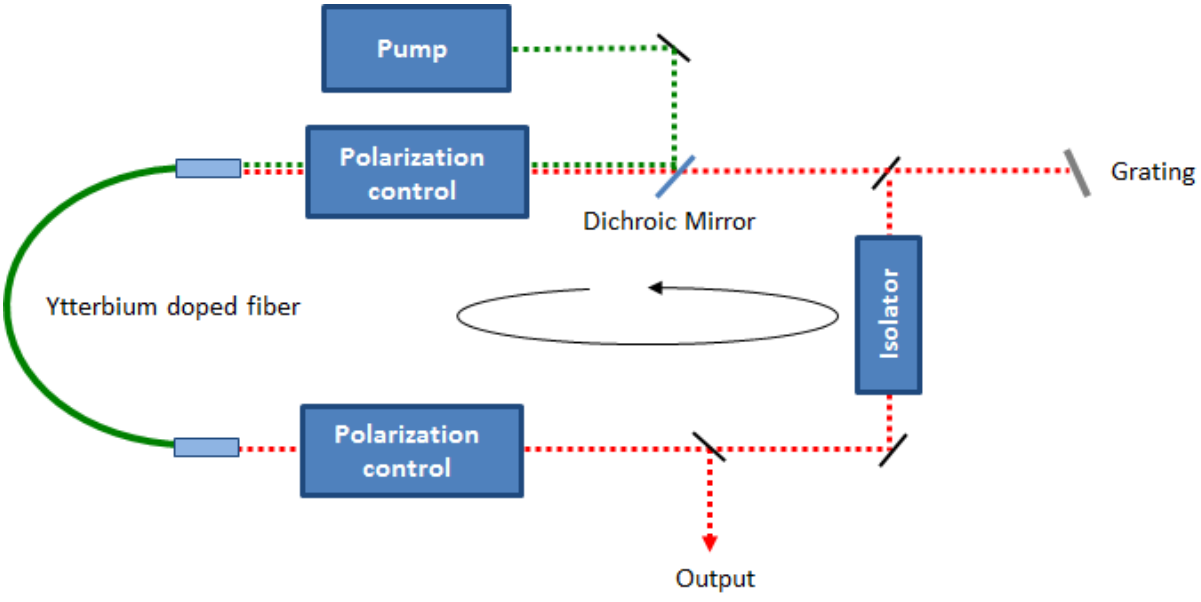

Fig. 1. All-normal dispersive setup of the oscillator. An isolating unit is stipulating the direction of the propagating laser light. A grating with 300 lines/mm assists the modelocking mechanism. The pumplight is coupled into the laser ring via a dichroic mirror.

The laser ring itself consists of a fiber which is highly doped with Ytterbium (Coractive SCF-YB550-4/125), offering an absorption of ~ 2600 dB/m at 974 nm, and a freespace-region. The latter includes quarter- and half-waveplates to tune the polarization states of the propagating light. Furthermore, a Faraday rotator in combination with two polarizing beamsplitters represents an isolator, stipulating the direction of the propagating light inside the cavity. The waveplates directly in front and behind the gain-fiber are electronically controlled via an in-house built driver-system. To achieve a maximum diffraction efficiency of the grating into the first order, another half-wavelength-plate in front of the grating is used to tune the polarization state of the incident light. For modematching of both sides of the gain fiber on the one hand and the pumplight side to the gain fiber on the other hand, adjustable collimators with lenses of a focal length of 4,5 mm were used. With a gainfiber of about 15 cm, the repetition rate of the oscillator, once modelocked, is 518 MHz (Fig. 2 (a).), according to an optical length of the cavity of ~ 58 cm. The degree of Laser efficiency is 42 % (Fig. 2. (b)), giving a maximum average output power of 380 mW when modelocked. The FWHM of the pulses is then 3,7 nm (Fig. 2. (c)).

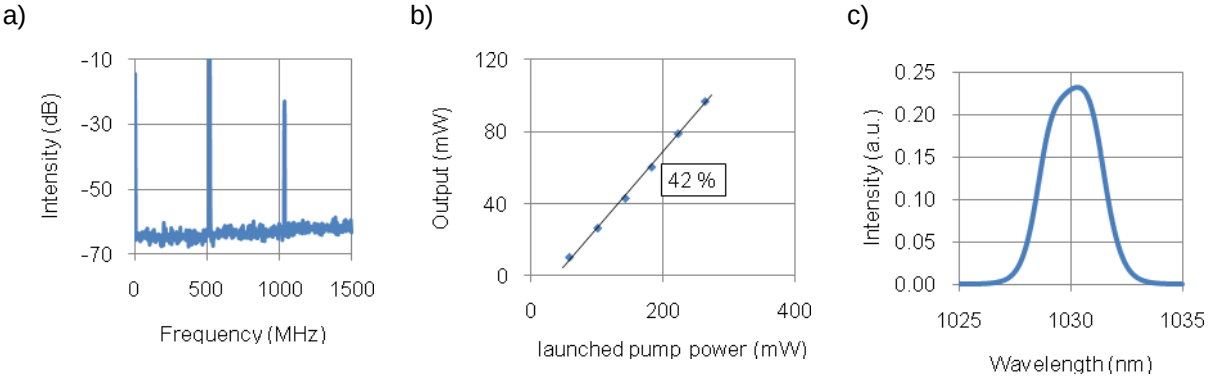

Fig. 2. Radio-frequency spectrum of the outcoupled pulses (a), degree of Laser efficiency of 42 % (b) and optical spectrum of the pulses while modelocked (c) with an FWHM of 3,7 nm.

In conclusion, the setup is quite compact with the given optical length of the cavity. Thereby, as stipulated in the work description T4.1 of this work package, a high repetition rate of 500 MHz can be achieved. High output powers of about 380 mW can be reached, combined with a high tunability of the emission center wavelength by tuning the angle of incidence of the backcoupled beam on the grating. However, the FWHM is not broad enough to satisfy the given requirements of an optical spectrum covering 1030 nm to 1060 nm wavelength.

A further approach to gain a broader spectrum is to illuminate less lines of the grating by focusing the light in the middle of the free-space area. It was possible to enhance the FWHM by this method by about 4 times to around 16 nm (Fig. 3.). The highest output power of ~ 380 mW is reached at a center wavelength of 1025 nm with respect to the higher emission cross section of the used ytterbium doped fiber at this wavelength.

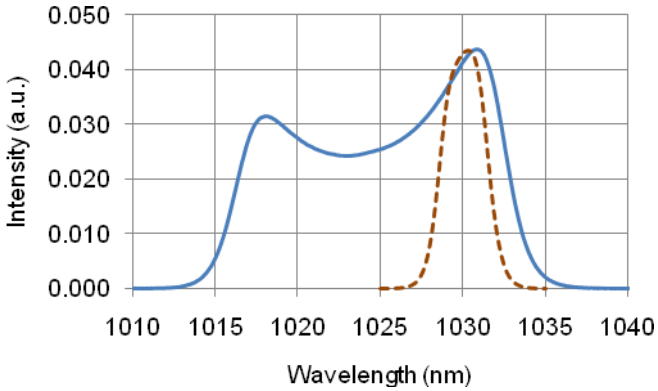

Fig. 3. Solid curve: Output spectrum of the modelocked high repetition rate laser. The FWHM is about 15 nm. Dashed curve: Optical spectrum for the all-collimated setup (see Fig. 2. (c)).

Although an increase of spectral bandwidth is possible by reducing the amount of illuminated lines on the grating, there is still a big gap on wavelengths so it is impossible to cover the range of 1030 nm and 1060 nm.

1.2. Laser setup with intra-cavity dispersion compensation

For further increase of the FWHM, one may also cancel the intracavity normal dispersion arising through the applied optics, allowing a maximum spectral broadening. This can be achieved by inserting a compressing unit, introducing anomalous dispersion into the ring. Instead of the single reflection grating, two transmission gratings in Littrow-Setup, in combination with a retroreflecting mirror for a double-pass configuration (Fig. 4) are used. The additional GVD is tunable between -6 fs² and -32 fs².

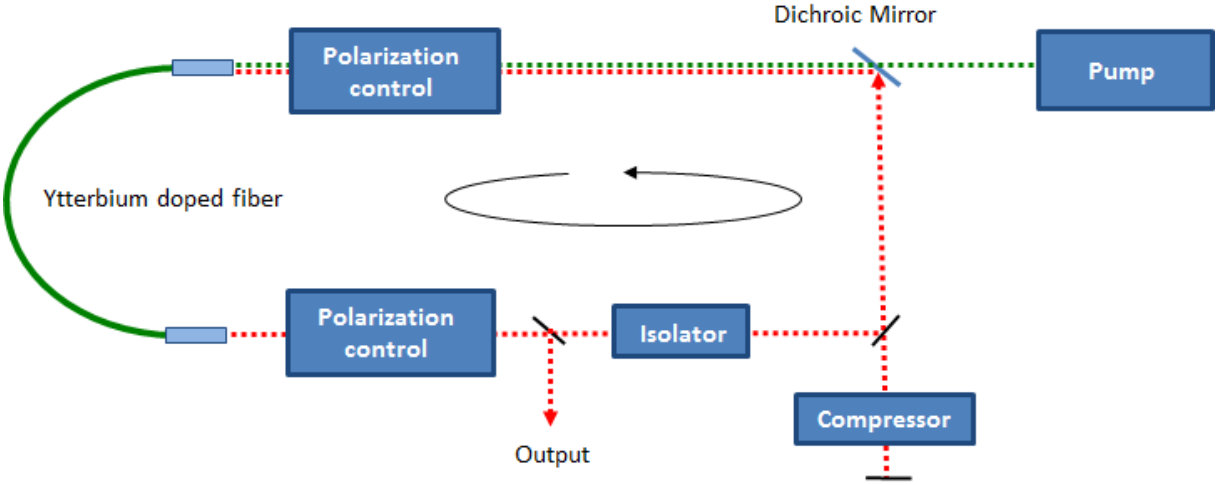

Fig. 4. Dispersion-compensated oscillator design. The grating compressor consists of two transmission gratings with 1000 lines /mm each and a retroreflecting mirror to ensure a double-pass configuration.

For a better way to handle the cavity and with respect to the upcoming packaging requirements, all of the adjustable collimators are replaced by fixed ones with pigtailed Hi1060 fiber, allowing a uniform modematching. By adjusting pump power and grating distance, and thus the intra cavity dispersion, mode locking can be observed in the normal dispersive (Fig. 5. (a)) and solitonic regime (Fig.5. (b)). In between these two operating regimes, the broadest spectra > 57 nm can be found (Fig. 5. (c)) delivering average output powers of > 200 mW. The threshold for the oscillator to form pulses with such broad spectra lies at average pump powers of ~ 760 mW. By fine adjustment, even modelocks with FWHMs of >80 nm can be found with respect to a lower average signal power, but still > 100 mW.

a) b) c)

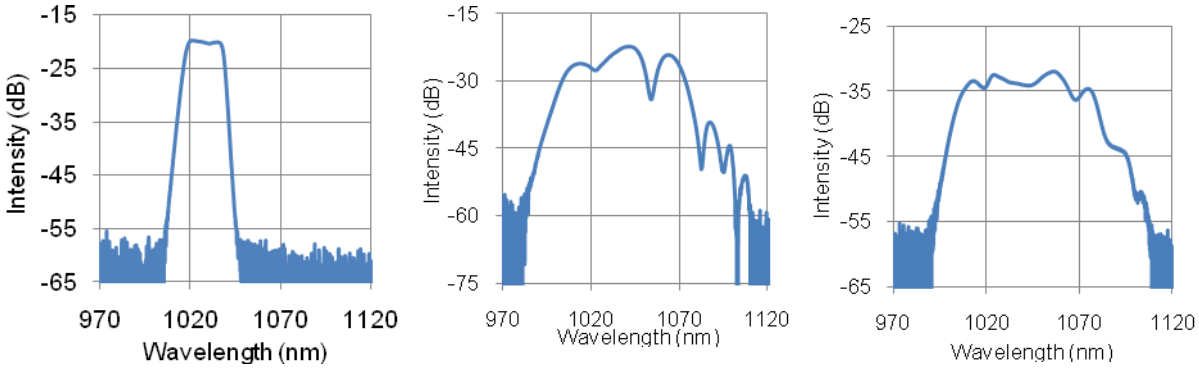

Fig. 5. Output spectrum of the modelocked laser in dispersion compensated setup in the normal dispersive regime (a) and in the solitonic regime (b). In between these to regimes, highest FWHMs can be reached > 57 nm (c).

In conclusion, by compensation for the intracavity normal dispersion, the oscillator reaches modelock states which cover a range of wavelengths from ~ 1020 nm to 1070 nm, as stipulated for the high power amplification for work description T4.3. By this, the optical requirements for the Master-oscillator for the upcoming processes in the context of WP4 of this project have been achieved. We have demonstrated a fiber-based oscillator, emitting pulses with ~ 500 MHz, covering a broad spectral range with average powers > 100 mW.

2. Packaging

To enable stable long term operation of this master oscillator the optimized optical design has been packaged into a robust enclosure (Fig. 6). The green line is showing the path of the pump light, in red the one of the intracavity beam. The outcoupled beam is pointed out as the blue line. The free space optical path length is only 25 cm. Accordingly the length of the fiber section is approx. 24cm. Taking into account the refractive index of the fiber this adds up to a total optical length of the resonator of 60 cm, as required for the 500 MHz repletion frequency. The repetition rate can be stabilized by use of a Piezo-driven end-mirror of the compressor unit. The design has been finished, all parts have been ordered. As soon as all parts have arrived the final laser system will be assembled.

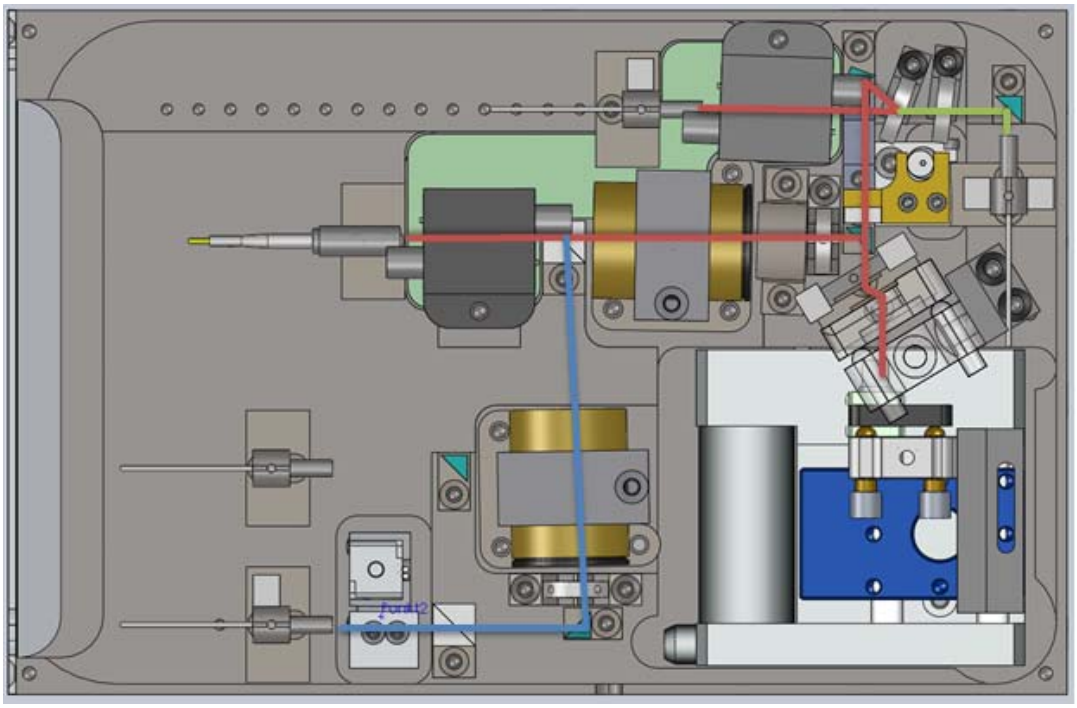

Fig. 6. Laserbox-Design of the 500 MHz oscillator. Basically the same optics as in the breadboard-setup are used, although due to better mechanical properties the cavity can be even more compact with a free-space optical length of only 25 cm.

3. General Conclusion and upcoming work

As part of work package 4 a master oscillator has been developed running at repetition rates as high as 500 MHz, as required in T4.1. The oscillator is able to emit pulses with FWHMs > 60 nm, to generate spectrally separated signals at 1030 nm and 1060 nm for the upcoming amplification as described in T4.3.for the future CARS-process. A robust package has been designed, although due to delivery-schedules not all parts have arrived yet, assembly and testing will be completed in the upcoming weeks.
By further reduction of the intracavity optical path length, even higher repetition rates of up to 750 MHz with broad spectra might be achievable, which might enhance the following CARS-process in view of the sampling rate.
Furthermore, although not needed in the course of this project enough space is provided to install elements for repetition-rate stabilization as well as on line dispersion-control, offering a high degree of control and flexibility.
For the future continuation of this project, the oscillator will be integrated in the high power amplification system, together with Bilkent University. Time line and specific tasks will be coordinated with the project partners.

CROSS TRAP WP4 Progress Report: Burst mode pulse picking and high power amplification of fs pulses

As a part of the high power fiber laser source to be used in CARS detection, a fiber amplifier system operating in the burst mode has been developed. Amplified signal bursts (macro pulses) containing pulses of energies as high as 27 µJ at a repetition rate of 1 kHz have been achieved. This progress report will consist of four main sections: A general description of the current state of the system, the development process and design considerations, end results and discussion, and future perspective.

1. General Description of the Current State of the System

The experimental system (Fig. 1) consists of an all-normal dispersion (ANDI) laser as the seed oscillator, two single-mode fiber pre-amplifiers, a double-clad (DC) fiber power amplifier and synchronized pulse picking and pulsed-pumping electronics.

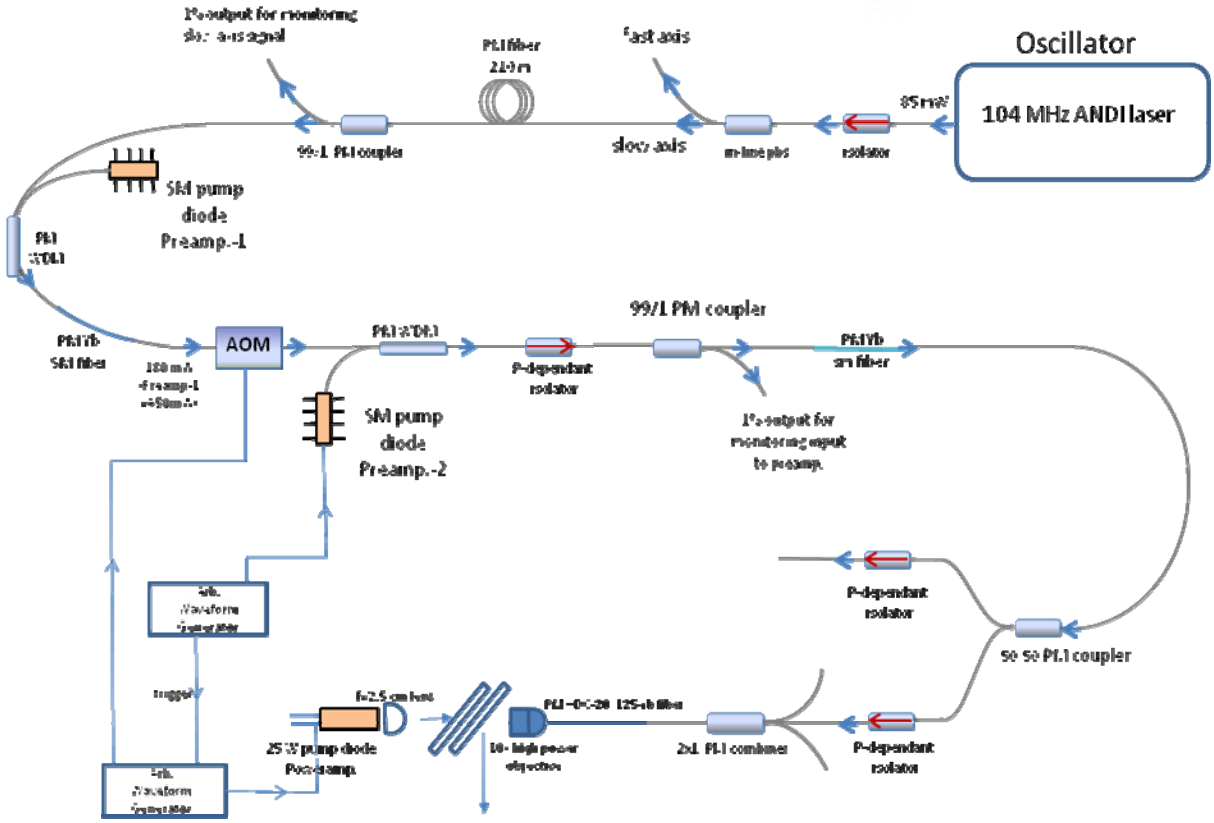

Fig. 1. Schematic diagram of the pulse burst amplifier system; WDM: wavelength division multiplexer; PBS: polarizing beam splitter; PM: polarization maintaining, SM: single-mode, DC: double-clad.

The fiber oscillator operates at a repetition rate of 104 MHz and outputs via a 40% output coupler an average power of 85 mW for a 18-nm wide output spectrum (Fig. 2. (a)) centered at 1030 nm. An isolator protects the oscillator from reflections from the rest of the amplifier system. The laser output is polarized with an inline polarization beam splitter, followed by polarization maintaining (PM) components. The slow axis output of the beam splitter which has a 19.5-nm wide spectrum (Fig. 2. (b)) is connected to the rest of the system. A 210-m long PM fiber placed after the polarization beam splitter stretches the pulses to 200 ps which was measured (Fig. 3(a)) by 25-GHz bandwidth detector and scanning oscilloscope combination.

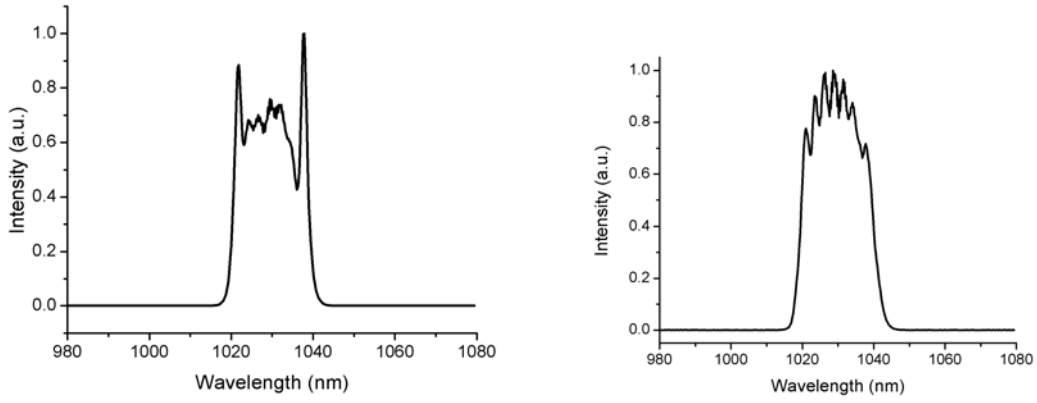

Fig. 2. Measured spectra of (a) oscillator output and (b) slow axis.

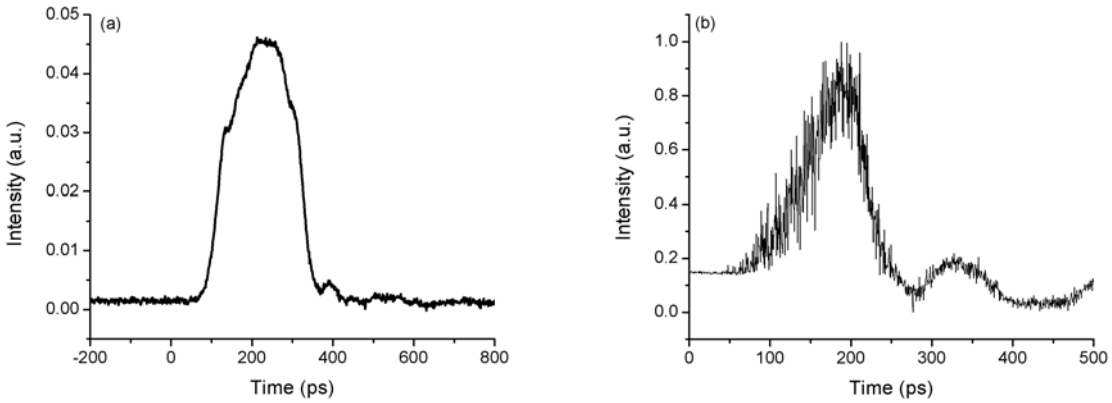

Fig. 3. Measured pulse duration (a) after the 210-m stretch fiber at full repetition rate of 104 MHz and (b) after the second preamplifier for a signal burst of 1 μs at 1 kHz, 130 μs pump pulse. The noise in (b) is due to the low repetition rate of 1 kHz.

The slow axis output of the beam splitter, which has dropped to 14 mW past the 99/1 monitoring port, is amplified by a preamplifier in the continuous mode to 180 mW with a pump power of 456 mW. A fiber-coupled acousto-optic modulator (AOM) placed after this preamplifier is used to obtain pulse bursts at desired repetition rates and with desired number of pulses. The pulse bursts are then amplified first with a second pre-amplifier operating in the pulsed-mode at a peak power of 500 mW. Pulse duration was measured at the output of the second preamplifier to be around 80 ps (Fig. 3(b)) for a signal burst of 1 μs, 100 μs pump pulse at a repetition rate of 1 kHz. The output of the second preamplifier is split by a 50/50 coupler before transmission to the power amplifier so that two separate amplified pulse bursts can be obtained for the synthesis of pump and Stokes pulses to be used in the standoff CARS detection scheme. Finally, in one of these arms, the pulses are amplified by a backward-pumped power amplifier also in pulsed-mode with a maximum peak pump power of 21.5 W. Two arbitrary waveform generators are used to drive the AOM and the pump diodes of the preamplifier and power amplifier, where the AOM gate and pump pulses are synchronized with adjustable relative delays. A polarization-dependant isolator is located at each output arm of the 50/50 coupler and after the pump diode of the second preamplifier. These isolators protect the pump diode of the second preamplifier from ASE formation in the second preamplifier and power amplifier which both operate in the pulsed mode. They further enhance the polarization extinction ratio (PER) of the signal beam. As a matter of fact, PER of the overall system output was measured to be above 20 dB at high levels of amplification. The PM pump combiner at the input of the power amplifier functions as a mode-field -adapter between the single-mode output of the isolator and double-clad Yb-fiber since it has a SM signal input and DC output.

For the power amplifier architecture free space backward pumping was used so that the gain fiber length could be chosen to minimize adverse effects of nonlinearity and keep the central wavelength around 1030 nm. Free space pumping made it possible to monitor the pump wavelength so that operation at 976 nm was possible by adjusting the temperature of the pump diode. Short length of the DC gain fiber (20/125 Yb 1200) was chosen to prevent signal spectrum broadening and drift towards higher wavelengths, and to minimize ASE formation under pulsed pumping. Since pulsed pumping made it possible to use significantly longer pump duration than the signal burst, the short gain fiber length favored energy storage using pump pulse with high peak pump power and long duration while lowering ASE production. Also backward pumping helped to obtain higher amplification of signal with shorter length of gain fiber. In the free space pumping configuration, two dichroic mirrors were used as a security measure to protect the pump diode against the signal beam. About

70% of the pump power was coupled into the gain fiber using the 10x high power objective and 2.5-cm focal-length collimating lens combination.

2. Development Process and Design Considerations

Burst-mode operation of a fiber amplifier system aiming high pulse energies at low burst repetition rates, relies on the principle of pump energy storage. For repetition rates lower than approximately 30-50 kHz, it is necessary to utilize pulsed pumping in order to avoid ASE generation between the pulse bursts. This operation mode requires detailed understanding of the gain dynamics to minimize ASE generation, while attaining high conversion efficiency. Hence, in the initial stage of development of our fiber amplifier system, the gain and ASE generation dynamics of the amplifier under pulsed pumping was characterized by investigating the pump-to-signal conversion efficiency, signal gain and amount of ASE formation, as a function of the pump pulse duration and the delay between the signal burst and pump pulse. At this early stage, the system (Fig. 4) consisted of the 104-MHz all-normal dispersion (ANDI) laser (mentioned above) as seed oscillator, an AOM for producing signal bursts followed by a single-mode fiber amplifier, and synchronized pulse picking and pulsed-pumping electronics.

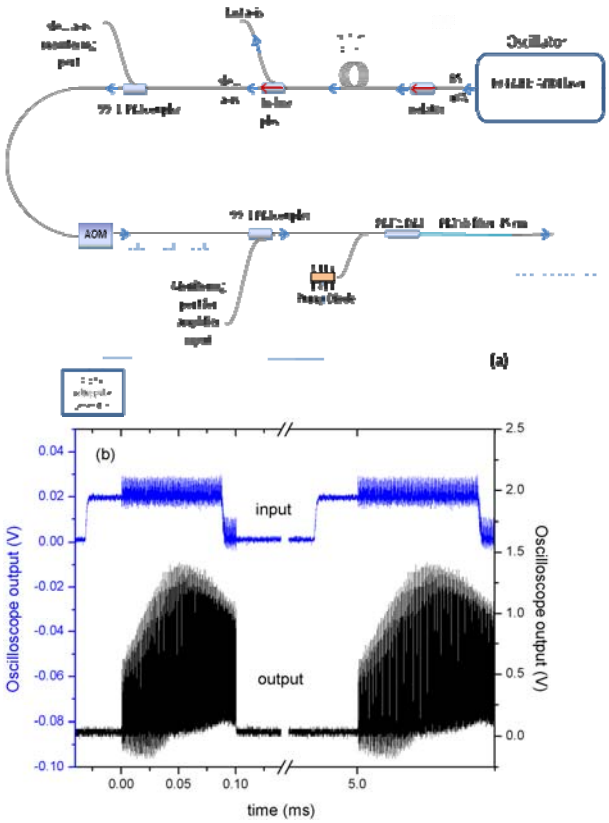

Fig. 4. (a) Schematic diagram of the experimental setup of the Yb-doped amplifier operating in the pulse-burst mode during the initial developmental stage. (b) Oscilloscope output of input and output pulse train (signal burst 100 µs, pump pulse 120 µs, signal lagging pump by 30 µs, rep. rate 200 Hz)

To begin with, the efficiency of the amplifier was measured in continuous pumping mode with no pulse picking as a benchmark for pulsed performance. In this mode, with 5 mW of signal power and 400 mW of pump power, amplified signal power was 200 mW, corresponding to a net gain of 16 dB and 50% pump-to-signal conversion. Input pulse energy for the amplifier was 50 pJ determined by the oscillator output and transmission of components up to the Yb fiber including the AOM. In the burst mode, the amplifier was operated with signal burst lengths of 20 µs and 100 µs at a repetition rate of 1 kHz and with 100 µs at 200 Hz. The lower limit of 20 µs for the burst mode duration was set by the

available signal power. These correspond to pulse bursts comprising of 2080 pulses repeated at 1 kHz (duty cycle of 2%) and 10800 pulses repeated at 200 Hz and 1 kHz (duty cycles of 2% and 10%, respectively). Reliable power measurements could be taken up to a maximum delay of 60 µs between pump pulse and signal burst since after this point unabsorbed pump power was observed in the spectrum of the amplifier output. The results of pump-to-signal power conversion measurements are shown in Fig. 5. For each signal burst duration, the conversion efficiency was measured as a function of the delay between rising edges of the pump and signal for different durations of the pump pulse. In the figures, each curve represents a different pump pulse duration denoted by the different duty cycles (pulse duration/pulse repetition rate). Comparing the three cases, the pump conversion efficiencies for 100 µs are significantly higher as a result of the fact that average signal power is well below saturation for the 20 µs case. Also the efficiency improves with increasing duty cycle for 100 µs going from 200 Hz to 1 kHz for the same reason. The results for 20 µs show that conversion efficiency increases with longer pump pulses and for each pump duration there is an optimum configuration where the falling edge of signal burst comes 10 µs after the falling edge of the pump pulse. For the 100-µs-long burst, the increase in conversion efficiency with the tested pump durations is more gradual with increasing duty cycle of the pump. This is due to the lower ratio of the pump duration to the signal burst length for this case, upper limit of which was dictated by the unabsorbed pump power.

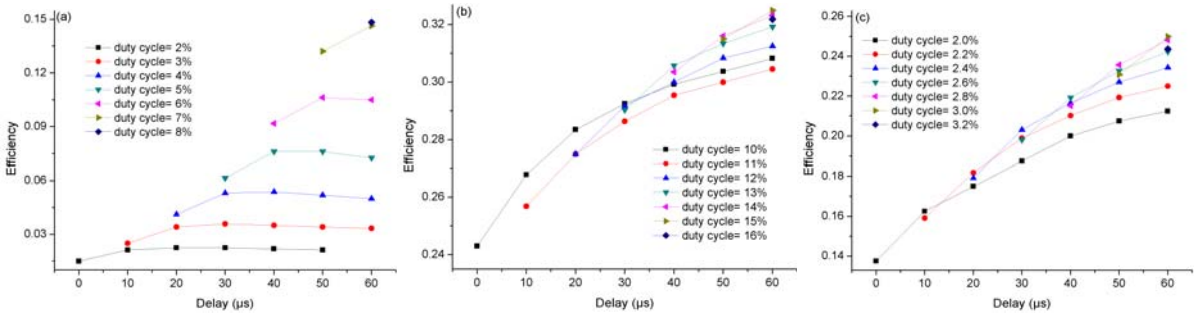

Fig. 5. Pump-to-signal conversion efficiency for pulse burst lengths of (a) 20 µs, (b) 100 µs at 1 kHz and (c) 100 µs at 200 Hz as a function of the delay between the rising edges of the pump and signal emissions for various pump duty cycles. The lines are only to guide the eye.

Fig. 6 (a)-(c) shows the levels of forward ASE produced in the pulse-burst amplifier, for signal bursts of 20 µs and 100 µs at 1 kHz, and 100 µs at 200 Hz, respectively. Since the power of ASE relative to the signal provides more relevant information than absolute power, the ratio of signal power to ASE power is given as a function of the delay between pump pulse and signal burst for different pump durations. The signal to ASE ratio is about 30 times higher for 100 µs burst duration at 1 kHz, and 20 times for 100 µs burst duration at 200 Hz, which is expected since the amount of forward ASE predominantly depends on the delay between the rising edges of the pump and signal. Thus, higher signal output levels for the longer signal burst significantly improves this ratio. This characteristic of ASE formation is demonstrated by the degrading signal to ASE ratio with increasing delay between pump and signal clearly observed in each case. The improvement in signal to ASE ratio with increasing pump duration is much stronger for the 20 µs signal burst due to the steeper increase in signal power with pump duration in this case as discussed in the above paragraph.

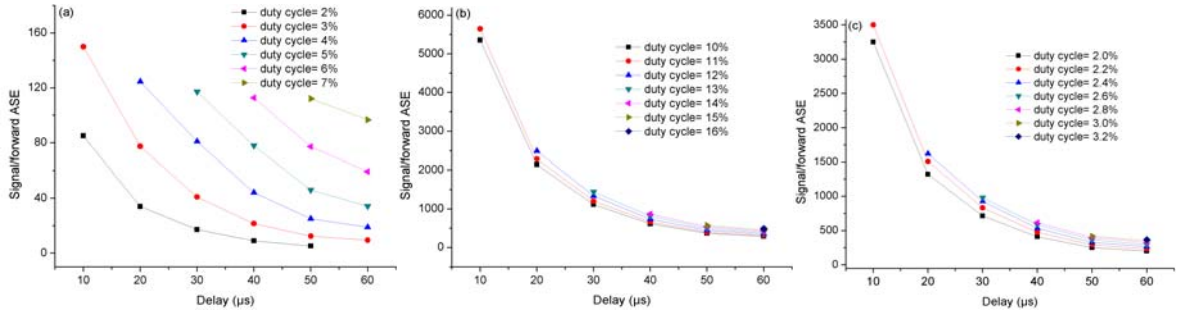

Fig. 6. The measured signal-to-ASE power ratio for pulse burst lengths of (a) 20 µs, (b) 100 µs at 1 kHz and (c) 100 µs at 200 Hz as a function of the delay between the rising edges of the pump and signal emissions for various pump duty cycles. The lines are only to guide the eye.

Amplifier gain for the pulse burst operation was also calculated in terms of the increase in energy per pulse. Results shown in Fig. 7, for 20 µs and 100 µs signal burst durations reveal a trend similar to the pump conversion efficiency. The increase with pump duty cycle in the shorter signal burst case is steeper as the pump pulse duration increase has a bigger impact in this case. The gain is lower than that (16 dB) of the continuous operation mode in general for all cases and it catches up for the longest pump pulse duration in each case. This indicates that the amplifier is running well below saturation due to low average signal power. The results also show that actual pulse energy gain can exceed the gain for continuous operation by increasing the available pump energy stored per signal pulse by using longer pump pulses.

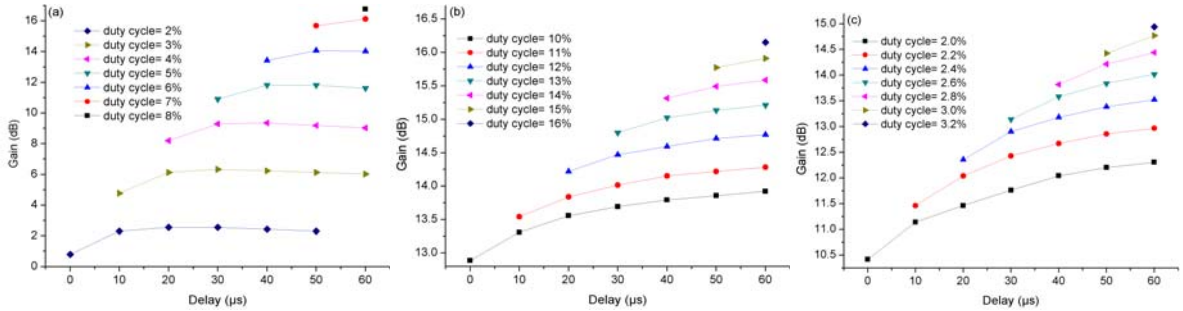

Fig. 7. The measured signal gain ratios for pulse burst lengths of (a) 20 µs, (b) 100 µs at 1 kHz and (c) 100 µs at 200 Hz as a function of the delay between the rising edges of the pump and signal emissions for various pump duty cycles. The lines are only to guide the eye.

The results of the initial investigation indicated that higher signal input power was needed for obtaining amplification at shorter burst durations, and in the burst mode amplification the peak pump power should be increased as much as possible before the pump duration to keep the ASE under control. As for the delay between signal burst and pump pulse, optimum condition occurred with signal burst coming after the pump pulse so that all of the pump energy is stored for the signal to consume. As a next step, a preamplifier was placed before the AOM which would work in the continuous mode and the input pulse energy was increased to 0.5 nJ level from 50 pJ by operating the pump at 370 mW. In the new configuration, pump-to-signal conversion efficiency, signal gain and amount of ASE formation was investigated as a function of signal burst duration since the final target for this system is to amplify short bursts and obtain high pulse energies. Fig. 8 (a)-(c) show the results of pump-to-signal conversion, signal gain and amount of ASE formation, respectively, as a function of signal burst duration for a pump pulse duration of 100 µs, peak pump power of 400 mW and repetition rate of 1 kHz. In these measurements, the delay between the signal and pump was adjusted such that falling edges of the signal burst and the pump pulse overlapped. The lowest signal burst duration used in the measurements was 1 µs, that meant about 100 pulses per burst which is a stipulation of the CROSS TRAP project. Note that the pump to signal conversion improved significantly compared to the previous case as a consequence of increased input power to the burst amplifier. It is evident that, although the pump-to-signal conversion for a 1 µs burst is less than half

of that for a 100 µs burst, the signal gain is 3.5 times more. This showed that significantly higher pulse energies can be obtained by keeping a high ratio of pump pulse to signal burst duration as long as the repetition rate allows and the ASE formation is kept under control. As a matter of fact, the measured signal to ASE ratio of 20 for the 1 µs burst was significantly low compared to that of 800 for the 50 µs burst, but still tolerable.

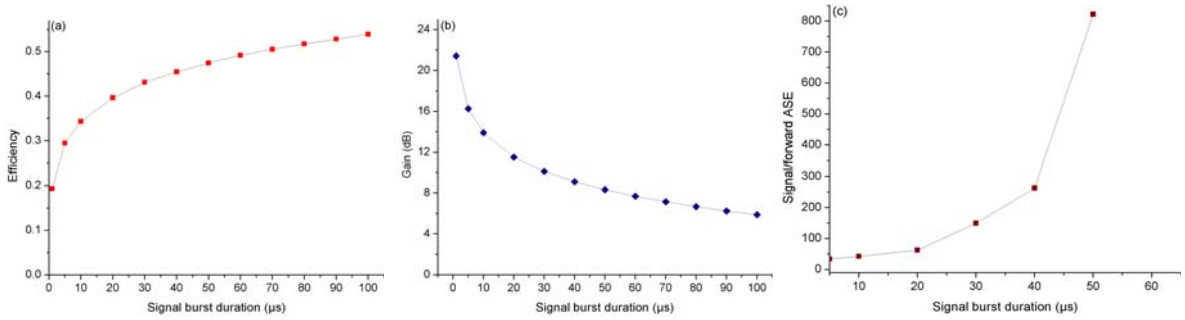

Fig. 8. The measured (a) pump-to-signal conversion efficiency, (b) signal gain factor and (c) ASE formation as a function of signal burst duration for a 100-µs pump pulse at a repetition rate of 1 kHz. The lines are only to guide the eye.

Next, burst mode amplification was investigated for a signal burst of 1 µs as a function of pump pulse duration, especially, since the CROSS TRAP project plan targets amplification of bursts made of some 100 pulses each, the precise value of which will be determined later. The measurements (Fig. 9) were taken as the pump pulse was varied from 10 to 100 µs, the peak pump power was again 400 mW and signal burst followed the pump pulse with falling edges overlapping. The results in Fig. 9 demonstrate a steep increase in the pump-to-signal conversion and signal gain as the pump pulse duration approaches 100 µs and also a tolerable signal to forward ASE ratio. Since it appeared like the system could handle longer pump pulses and higher amplification could be achieved, next an isolator was placed after the preamplifier diode operating in the pulsed mode as a precaution against backward ASE which is stronger than forward ASE and which would further increase with longer pump pulse duration.

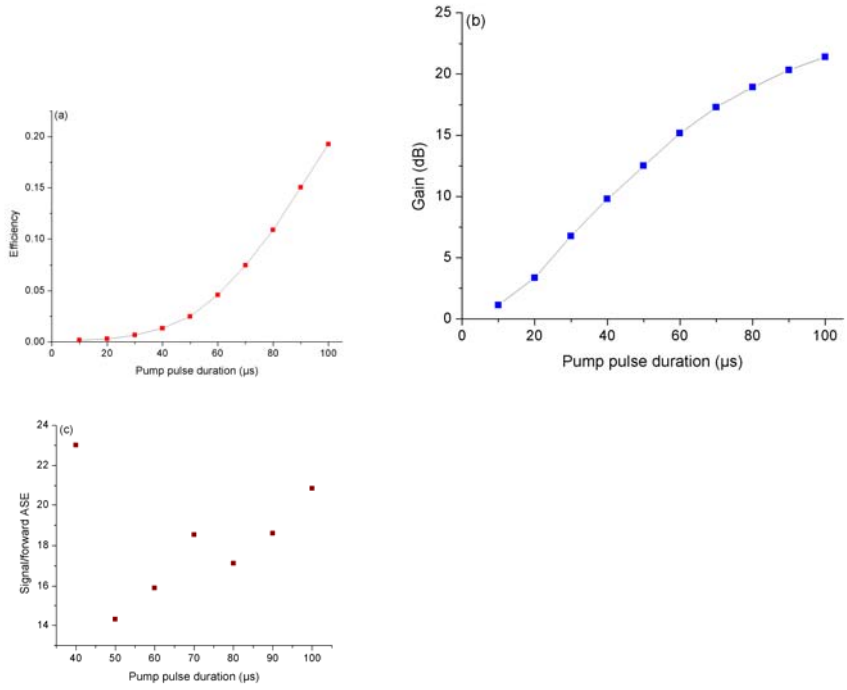

Fig. 9. The measured (a) pump-to-signal conversion efficiency, (b) signal gain factor and (c) ASE formation as a function of pump pulse duration for a 1-µs signal burst at a repetition rate of 1 kHz. The lines are only to guide the eye.

This time the pump power of the preamplifier before the AOM was increased to 450 mW, close to maximum available power, to compensate for the loss of the added isolator at the input of the burst-mode preamplifier. Also the burst-mode preamplifier was operated at the maximum possible peak pump power of 510 mW, in order to obtain maximum amplification in the system. When the pump pulse duration is increased further, the optimum pulse amplification occurs about a pump duration of 130 µs as the results in Fig. 10 indicate. For longer pump pulse durations, the pump-to signal conversion deteriorates due to unabsorbed pump power mainly which also worsens the signal-to-ASE ratio by stagnating the signal gain.

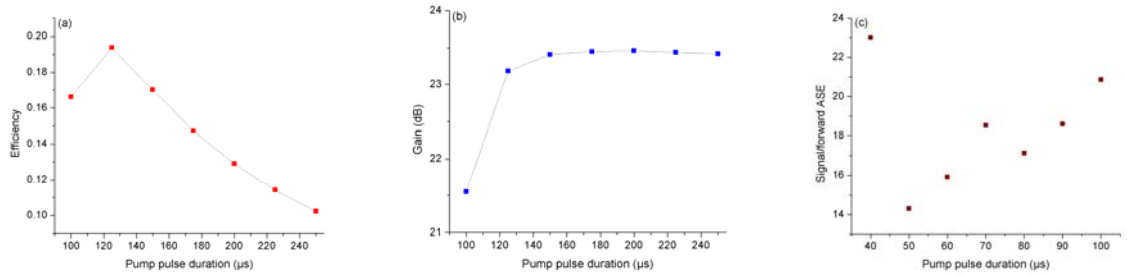

Fig. 10. The measured (a) pump-to-signal conversion efficiency, (b) signal gain factor and (c) ASE formation vs. pump pulse duration from 100 to 250 µs for a 1-µs signal burst at a repetition rate of 1 kHz. The lines are only to guide the eye.

So at this stage of the development process, optimum amplification condition for targeted burst mode was identified and the system could produce a maximum pulse energy of 120 nJ for 1 µs signal bursts containing around 100 pulses at a repetition rate of 1 kHz. The next step was to add a power amplifier to the system to amplify pulses further up to the 5 – 10 µJ level. However, before the power amplifier could be added the output of the second preamplifier had to be split in two arms with a 50/50 coupler to synthesize pump and Stokes signals separately for the CARS detection scheme and then a polarization dependant high power isolator was placed in each arm to protect the preamplifier (burst-mode) from reflections and ASE from the power amplifier. Due to the insertion loss of the added components and splitting of the signal, the signal power was reduced to nearly one fourth of the second preamplifier output. Hence, at the power amplifier input, a pulse energy of around 30 nJ was obtained for a 1 µs signal burst. Meanwhile, a favorable effect of the isolators was to improve the signal-to-forward ASE ratio by reducing the initially unpolarized ASE to half its power level at the output of the preamplifier by polarization selection. Therefore, the actual signal-to-forward ASE ratios at the input of the power amplifier would be twice of those data shown in Figs. 8-10 (c).

Based on our experience on the burst amplification system so far, backward pumping seemed much more suitable for the arm of the amplifier system which would provide the narrow bandwidth pump pulses centered around 1030 nm. Backward pumping would make it possible to keep the gain fiber (PM-DC-Yb fiber with 20 µm core diameter and 125 µm cladding diameter) short to hinder spectral broadening and other effects due to nonlinearity such as Raman scattering to occur and avert drifting of the signal spectrum to longer wavelengths. It was also critical to operate the pump diode at 976 nm, to maximize pump absorption and hence keep the Yb fiber length as short as possible. In this aspect, free space pumping with dichroic mirrors made it possible to monitor the pump wavelength and maintain it at 976 nm by adjusting the diode temperature.

3. End Results and Discussion

When the system was operated in the burst mode at a repetition rate of 1 kHz, highest average pulse energy of 17 µJ was obtained for a burst duration of 150 ns which contained

an average of 16 pulses. In this case, the pump pulse duration for the second preamplifier and the power amplifier was 135 µs and 130 µs, respectively. The pump diode of the first preamplifier (continuous mode)was operated at 450 mW and of the second one (burst mode) at 500 mW peak power, near to the maximum available levels. The delays between rising edges of the pump and signal pulses were adjusted to maximize output pulse energy. Since the earlier pulses get amplified more compared to the latter ones, a rising ramp pulse was applied to the AOM to obtain an output burst with a uniform pulse distribution as possible. The input and output pulse burst, and the spectrum of the output signal is shown in Fig. 11. The energy of the highest-energy pulse in the burst was calculated to be 27 µJ. The average output power of 270 mW, which meant a signal burst energy of 270 µJ, indicated a pump-to-signal conversion of 14 % in the power amplifier considering the average pump power of 2.8 W, 70% pump coupling ratio and 13 % duty cycle. The gain achieved in the power amplifier is 23 dB with the input signal power of 1.4 mW, input pulse energy of 90 nJ. The measured output spectrum (Fig. 11 (b)) shows that no broadening or drift towards longer wavelengths occurs and ASE formation is negligible.

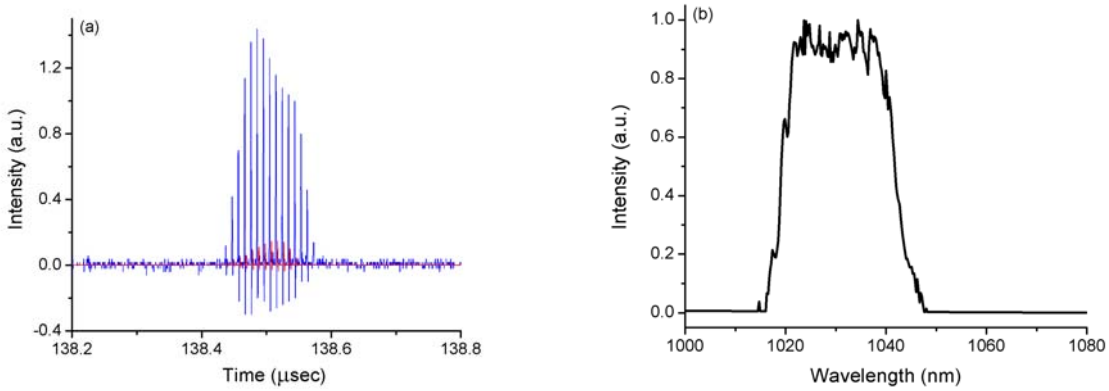

Fig. 11. (a) Output (blue line) and Input (red line) pulse train, (b) output spectrum for 150 ns signal burst, output power of 270 mW, average output pulse energy of 17.3 µJ, highest pulse energy of 27 µJ.

Also signal bursts of 1 µs (around 100 pulses per burst) were amplified at a repetition rate of 1 kHz and identical pumping conditions as in the 150 ns burst case (except slight adjustment of delays) with various ramp gate signals applied to the AOM. The resulting pulse trains and output spectra for two different ramp signals are shown in Fig. 12. In both cases, nearly the same average pulse energy of 3.4 µJ was obtained; while, the maximum pulse energy reached 14 µJ in the first case with highly nonuniform pulse distribution (Fig. 12(a)), while it was 5.5 µJ for the more uniform case of Fig. 12(c). The system produced an average power of 350 and 345 mW for the two cases, respectively, for an average pump power of 2.8 W provided by the power amplifier diode. The spectra show that in both cases ASE formation and nonlinear effects were negligible and the central wavelength is around 1030 nm.

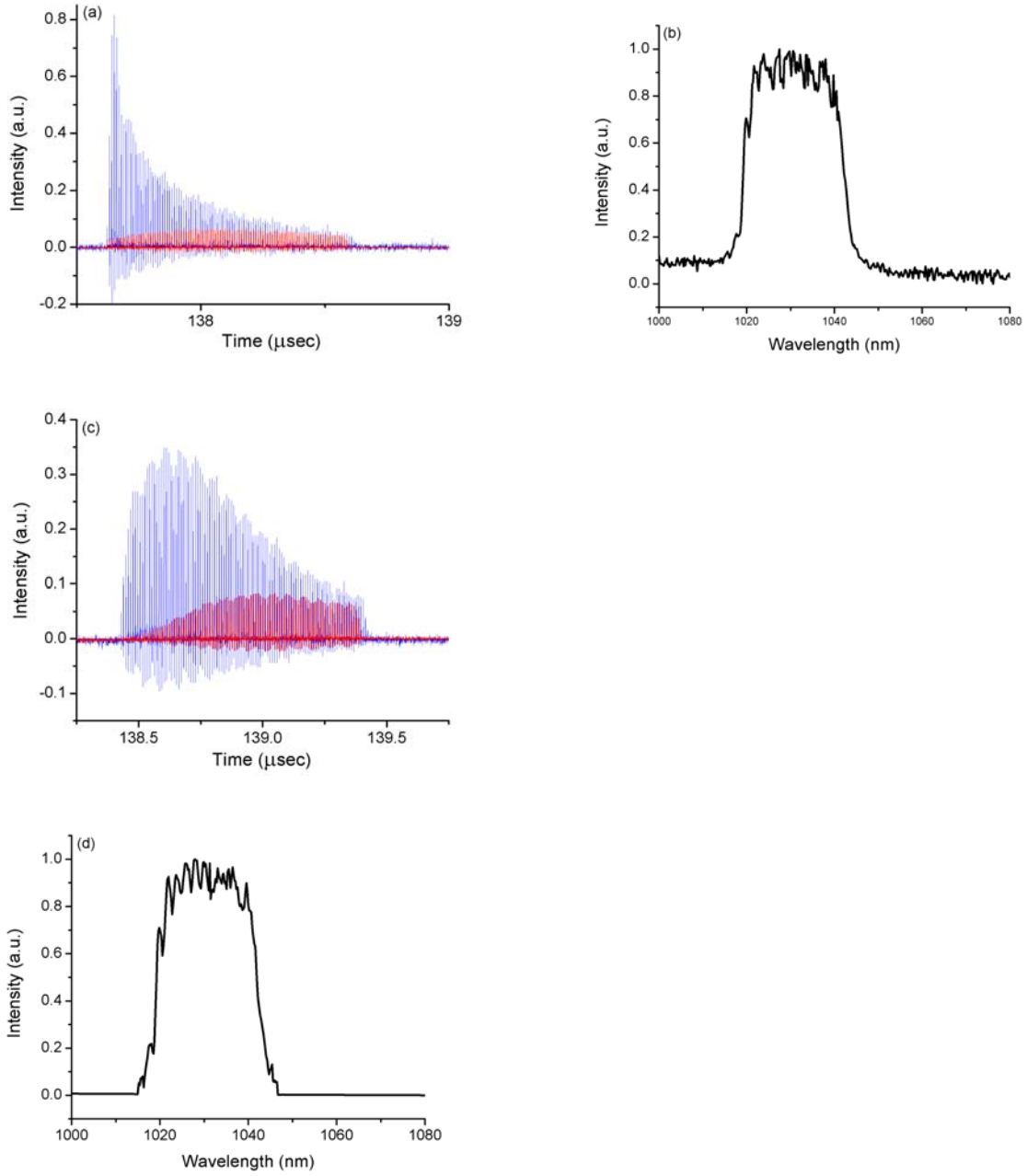

Fig. 12. Output (blue line) - Input (red line) pulse trains ((a) and (c)), and corresponding output spectra ((b) and (d)), respectively, for two different 1-µs signal bursts at a repetition rate of 1 kHz.

Further pulse amplification measurements were done with burst durations of 0.5 and 10 µs, containing around 50 and 1000 pulses per burst, at 1 kHz and identical pumping conditions except, again, for slight adjustments of the delays between signal burst and pump pulses. The results are shown collectively in Fig. 13. The outcome is clearly in parallel with those of the preamplifier in Fig. 8, except that the pump-to-signal conversion efficiency for 10 µs burst is significantly lower. This is probably due to the short length of gain fiber which favors amplification of short bursts where earlier arriving pulses consume the stored gain in the Yb-fiber.

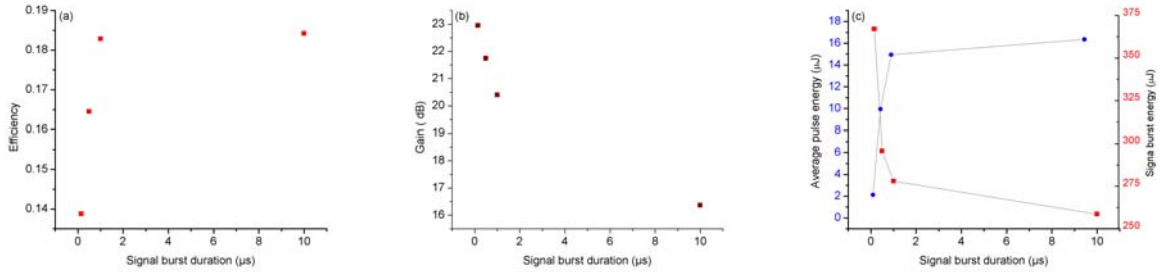

Fig. 13. Power amplifier high pulse energy results: (a) pump-to-signal conversion, (b) signal gain and (c) average pulse energy (red squares) and energy contained in a signal burst (blue circcles) at 1 kHz, 2.8 W average pump power, 130 µs pump pulse duration. The lines are only to guide the eye.

Finally, amplified pulses of highest energy (20 µJ) achieved in the system were compressed to 500 fs by a grating compressor pair. Since autocorrelation measurement at 1 kHz was not possible due to the limit of the autocorrelator, pulse picking at 10 kHz was used and 10 ns gate signals were applied to the AOM. AOM transmitted around 3.3 pulses per pick since it had a rise/fall time of 30 ns. Hence, operating the amplifier system at an output power of 660 mW output power at 10 kHz repetition rate, pulses of 20 µJ average energy were obtained. The autocorrelation result together with the output pulse train per pick and output spectrum are given in Fig. 14.

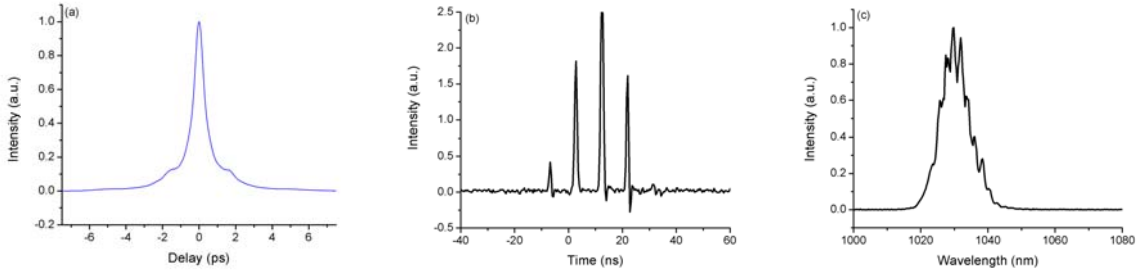

Fig. 14. (a) Autocorrelation result, (b) output pulse train per pick which was repeated at 10 kHz (c) output spectrum for the amplified pulses of 20 µJ average energy that were compressed to 500 fs.

4. Future perspective

Continuation of the project work includes testing of higher pulse energies with the currently set-up power amplifier by increasing the pump capacity, constructing a power amplifier for the second output arm of the system, integration of the high-repetition rate oscillator which will be delivered by Menlo Systems and cooperation with POLIMI to synthesize tunable narrow-bandwidth pump and Stokes pulses. In addition transportability of the system has to be improved by some further packaging effort. The specific path of the continuation work will be determined in coordination with the project partners.